SEA ICE CONCENTRATION AND SEA ICE EXTENT MAPPING WITH THE FSSCAT MISSION: A NEURAL NETWORK APPROACH

David Llaveria[1], Juan Francesc Munoz-Martin[1], Christoph Herbert[1,3], Miriam Pablos[2,3], Adriano Camps[1,3], Hyuk Park[1]

[1] CommSensLab Unidad María de Maeztu - Dept. of Signal Theory and Communications, Universitat Politècnica de Catalunya and IEEC/CTE-UPC
[2]Physical and Technological Oceanography Group, Institut de Ciències del Mar, Consejo Superior de Investigaciones Científicas (ICM-CSIC)
[3] Barcelona Expert Centre (BEC) on Remote Sensing
Email: david.llaveria@upc.edu.

ABSTRACT

Knowledge about sea ice concentration and extent in polar regions is of great interest both for economic interests, and as a proxy of the climate change. Retrieved maps are based on data from microwave radiometers, which are currently provided by large satellite missions. Nowadays, CubeSats have proven to be a cost-effective alternative. Due to their low cost, they can be launched in large constellations to obtain high spatial coverage and daily revisit. This study presents a neural network approach to generate sea ice concentration and sea ice extension maps using the L-band microwave radiometer, and the GNSS-Reflectometer data from the FMPL-2 instrument onboard [3]Cat-5/A, one of the two CubeSats of the FSSCat mission. The results obtained during the first 2 months of the mission are presented.

Index Terms— CubeSat, Sea ice concentration, Sea ice extent, Neural Networks

1. INTRODUCTION

Polar sea ice is declining due to the global temperature increase. Although this evidences a real global problem, it also opens new commercial routes through the Arctic Ocean. There are obvious commercial interests as the North route from China to Western countries, which is about two weeks shorter than that through the Indian Ocean and the Suez canal. Therefore, knowing the actual ice extension to either define these routes or to monitor the effects of climate change is a major concern. Today's maps are generated by different Earth Observation missions using large satellites, such as microwave radiometers, synthetic aperture radars, or even optical imagers in cloud-free conditions. As a cost-effective alternative, the FSSCat demonstration mission [1,2] was launched in September the 3rd, 2020 in the Vega Proof of Concept (PoC) for Small Satellite Mission Service (SSMS). The main objective of this mission is to monitor the sea ice over the poles. FSSCat is composed by two 6U CubeSats. One of them embarks the FMPL-2 payload [3,4], a dual instrument with an L-band Microwave Radiometer (MWR), and a Global Navigation Satellite System-Reflectometer (GNSS-R), both implemented using a Software Defined Radio.

Previously, the use of matched filters to obtain the Delay Dopler Maps (DDM) [5] in combination with Neural Networks (NN)-based algorithm [6] has proven to be a fast and reliable approach to retrieve sea ice concentration using data from the TechDemoSat-1 (TDS-1) satellite. This study proposes a NN-based methodology to estimate Sea-Ice Concentration (SIC) and Sea Ice Extension (SIE) maps using data from the two FMPL-2 sensors: the L-band MWR, and the GNSS-R.

2. SEA-ICE MAPPING

In order to generate the SIC and the SIE maps, a two-step methodology is used. Firstly, full maps of the Arctic and the Antarctic seas are generated at a coarse resolution using MWR brightness temperature data. Later, the corresponding GNSS-R data points are superimposed to the resulting maps of the first step to improve their spatial resolution. In both steps, similar NN are used to process the data and generate the outputs, either the continuous SIC or the binary SIE. FSSCat mission is delivering data since early October. In this research, data acquired during October and November (2 months) have been processed using this methodology. All NNs have been trained using SIC maps provided by Ocean and Sea Ice Satellite Application Facility (OSI SAF) as ground truth [7]. A percentage of the available data has been used to train the NNs; less than 2% of the MWR data (roughly 20,000 samples), and a 70% of the samples for the GNSS-R case due to the smaller dataset available.

2.1. Microwave radiometer maps

The NN employed to produce the SIC maps from the MWR data includes a regression fit network with 3 hidden layers composed by 5, 10 and 5 neurons, respectively. It has 5 inputs consisting of:

i) the brightness temperature (Ta) measured by the MWR;
ii) the standard deviation of Ta;
iii) the bidimensional gradient of Ta;
iv) the percentage of Land Cover within the antenna footprint (350 x 500 km^2);
v) the land and sea surface temperature (skin temperature) from the European Centre for Medium-Range Weather Forecasts (ECMWF) model [8].

To generate the sea ice extension maps, a binary classification NN is used. The network is composed by a single hidden layer with 10 neurons. The inputs are the same as in the sea ice concentration case.

Brightness temperature maps are obtained based on previously averaged daily tracks of MWR data, which are spatially interpolated according to the MWR antenna pattern and projected on a 12.5 km Equal-Area Scalable Earth Grid (EASE-Grid 2.0) [9].

2.2. GNSS-R maps

The GNSS-R maps are generated using the identical NN used for MWR, except for the inputs. In that case, 6 Inputs are used:

i) the DDM integrated in the delay dimension the standard deviation of Ta;
ii) the reflectivity;
iii) the signal-to-noise ratio of the measurement;
iv) the elevation angle during the capture;
v) the azimuth angle during the capture;
vi) the temperature measured with the MWR.

In this case, the GNSS-R resolution is finer (i.e., the size of the Fresnel zone ~500 m) thanks to the very short integration time [4]. Thus, the data is delivered in a scattered format instead of gridding it into a 12.5 km grid in order to preserve the high resolution. The MWR measurements and the OSI SAF data are scattered into the specular point location using a 2D linear interpolation.

3. RESULTS

The performance of each model was analyzed over the Arctic and the Antarctic seas. In Figure **1**, a weekly composite of Arctic SIC maps from November 6 to 12, 2020 is presented, using MWR data (a) and OSI SAF (b). In general, both SIC maps display similar spatial patterns. Nevertheless, most of the discrepancies are located at the lower-concentrated sea ice margin along coastal areas. Table I shows the errors between the estimated SIC using the MWR data and the OSI SAF reference. The mean absolute error is lower than 6% for the Arctic, while for the Antarctic it is lower than 5%. The error standard deviations are around 13% and 11%, respectively. Therefore, errors in Arctic are always larger than those in Antarctic. This can be explained because there are more land-ice-sea transitions in the Arctic than in the Antarctic, where the ice is forming a huge mass surrounding the land.

Regarding the SIE maps, the accuracy using the MWR data is larger than 93% in the Arctic, and larger than 96% in the Antarctic. For the GNSS-R data the accuracy depends on the quality of the included data points. Lower average SNR in the track reduces the estimation accuracy. However, the number of points decreases as the track average SNR increases due to filtering out some of the data. The accuracy ranges from 95% to 97%, selecting the tracks with an 2.5 dB or 3.2 dB averaged SNR, respectively.

The Antarctic SIE maps generated from MWR data are presented in Figure 2, showing the estimations (a) and the ground truth (b) obtained in a three-day period from November 19 to 21, 2020. Similar to the results obtained during the estimation of SIC, it can be seen that the classification errors usually occur in the borders of the ice. Although the grid size is 12.5 km, as mentioned in section 2, the real footprint of the radiometer antenna is 350 x 500 km^2. Therefore, the generated maps using MWR data are blurrier than the OSI SAF ones used as ground truth.

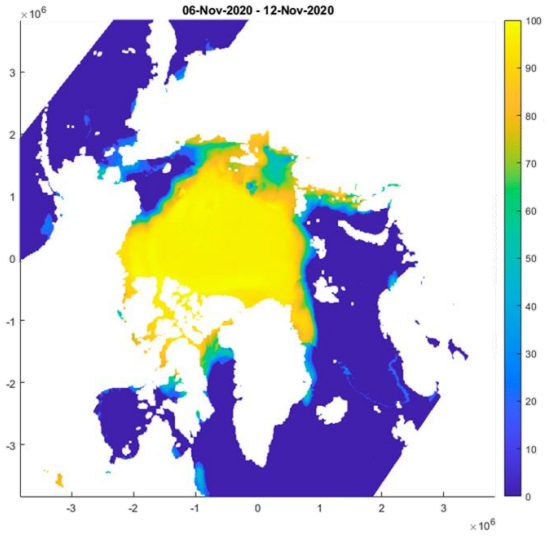

Figure 1. Arctic SIC map: a) Generated using FSSCAT MWR data, b) OSI SAF Ground Truth

TABLE I
MWR SEA-ICE CONCENTRATION ERRORS COMPARED TO GT

	Mean absolute Error	Error STD
Arctic	5.8%	13.2%
Antarctic	4.9%	11.1%

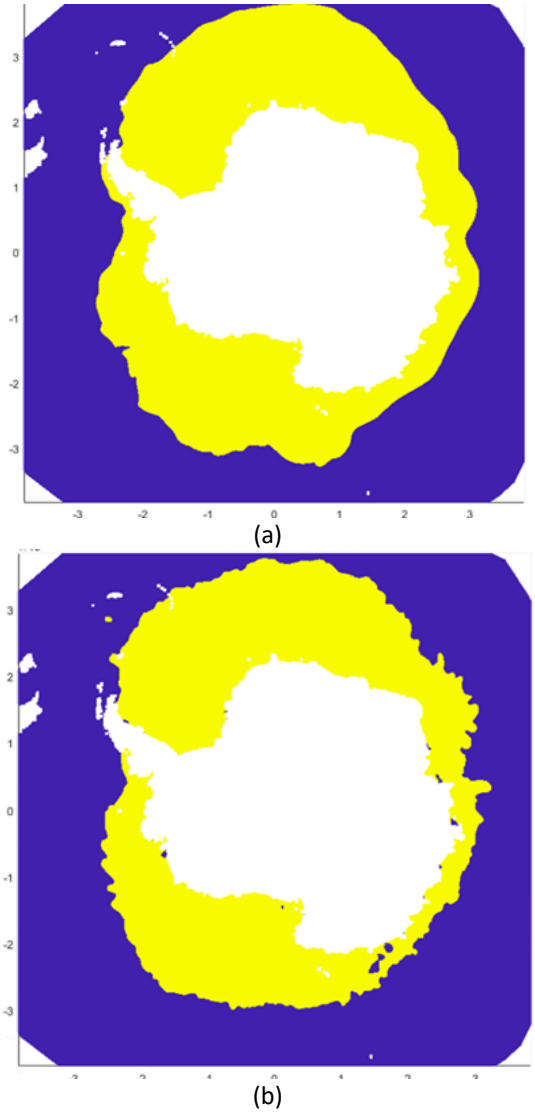

Figure 2. Antarctic SIE map: a) Generated using FSSCAT MWR data, b) OSI SAF Ground Truth. Blue indicates open water and yellow refers to sea ice.

Figure **3** shows the GNSS-R tracks after being processed by the classification NN. The points in orange are the ones detected as ice, and the points in turquoise color are those detected as water. Ground truth SIC data are highlighted in blue color. Brighter tones represent SIC ranges between 15% and 30% and values larger than 30%, respectively, and dark blue indicates the sea. It can be seen that the GNSS-R clearly detects some transitions that are not captured in MWR-based model due to the coarse resolution, as the sea lake located at the top center part of the image (inside the red square). As in the MWR case, the errors are given in some of the transitions due to the heterogeneity of the ice in the lower concentration areas, although these uncertainties might also be introduced by the poorer spatial resolution of the OSI SAF product (10 km).

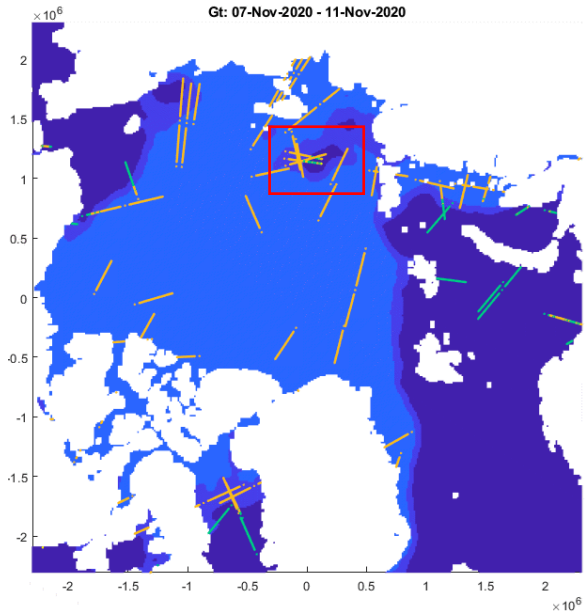

Figure 3. GNSS-R tracks superposed to OSI SAF ground truth.

The total areal extension of sea ice at both poles is determined from the SIE maps, and the corresponding time series are presented in Figure 4 from the beginning of October to mid-November 2020. The difference with respect to the total extension area from OSI SAF is similar to the differences between existing sea ice extension products [10].

4. CONCLUSIONS

In this work, a new method to generate full SIC and SIE maps of the Arctic sea and Antarctic ocean is presented. This methodology uses data from the FMPL-2, a payload carrying a combined microwave radiometer, and a GNSS-Reflectometer onboard the ^{3}Cat-5/A satellite of the FSSCat mission. SIC and SIE maps are constructed using a two-step approach. Coarse maps are first generated based on MWR brightness temperature data. These maps are then complemented by high-resolution GNSS-R data in areas, where specular reflection occurs, and values can be provided. In all cases, the error is under 6%. Looking at the total extension area, the errors are similar to those obtained from existing sea ice products.

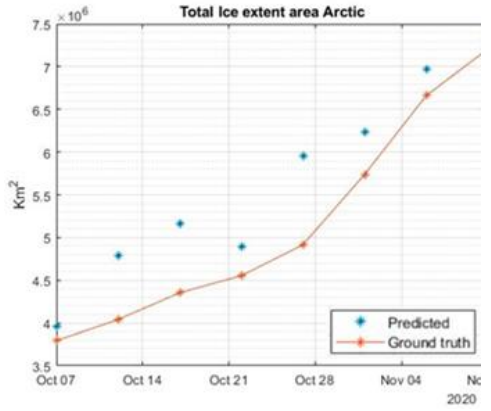

(a)

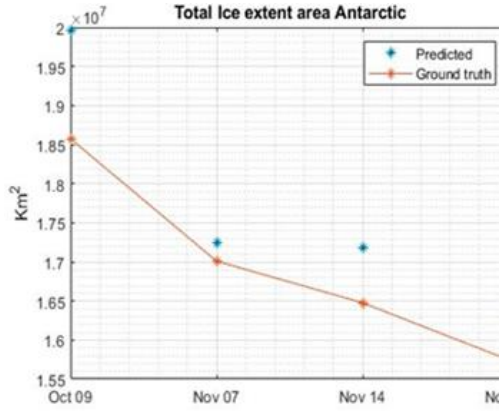

(b)

Figure 4. Total SIE of a) the Arctic and b) the Antarctic.

ACKNOWLEDGEMENTS

This project has been sponsored by the 2017 ESA S3 challenge and Copernicus Masters overall winner award ("FSSCat" project), by the Spanish Ministry of Science, Innovation and Universities, "Sensing with Pioneering Opportunistic Techniques", grant RTI2018-099008-B-C21 / AEI / 10.13039/501100011033, and ESP2017-89463-C3 project, by "CommSensLab" Excellence Research Unit Maria de Maeztu (MINECO grant MDM-2016-0600), by a FPU fellowship from the Spanish Ministry of Education, by the Centro de Excelencia Severo Ochoa (CEX2019-000928-S), and by the CSIC Plataforma Temática Interdisciplinar de Teledetección (PTI-Teledetect).

Christoph Herbert was supported by a fellowship from "la Caixa" Foundation (ID 100010434) with the fellowship code LCF/BQ/DI18/11660050, and has received funding from the European Union's Horizon 2020 research and innovation programm under the Marie Sklodowska-Curie grant agreement No. 713673.

REFERENCES

[1] A. Camps et al., "FSSCat, the 2017 Copernicus Masters' "Esa Sentinel Small Satellite Challenge" Winner: A Federated Polar and Soil Moisture Tandem Mission Based on 6U Cubesats," *IGARSS 2018 - 2018 IEEE International Geoscience and Remote Sensing Symposium*, Valencia, 2018, pp. 8285-8287, doi: 10.1109/IGARSS.2018.8518405.

[2] A. Camps, J.F. Muñoz-Martin, J.A. Ruiz-de-Azúa, L. Fernández, A. Pérez-Portero, D. Llavería, C. Herbert, M. Pablos, A. Golkar, A. Gutiérrrez, S. Briatore, N. Garzaniti, F. Nichele, R. Mozzillo, A. Piumatti, M. Cardi, M. Esposito, B. Carnicero, M. Pastena, G. Filippazzo, A. Reagan, "FSSCAT Mission Description and First Scientific Results of the FMPL-2 Onboard 3Cat-5/A" *IGARSS 2021 - 2021 IEEE International Geoscience and Remote Sensing Symposium.* [submitted for publication]

[3] J. F. Munoz-Martin, L. F. Capon, J. A. Ruiz-de-Azua and A. Camps, "The Flexible Microwave Payload-2: A SDR-Based GNSS-Reflectometer and L-Band Radiometer for CubeSats," in *IEEE Journal of Selected Topics in Applied Earth Observations and Remote Sensing*, vol. 13, pp. 1298-1311, 2020, doi: 10.1109/JSTARS.2020.2977959.

[4] J. F. Munoz-Martin. L. Fernandez, A. Perez, J.A. Ruiz-de-Azua, H. Park, A. Camps, B.C. Domínguez, M. Pastena, 2021. "In-Orbit Validation of the FMPL-2 Instrument—The GNSS-R and L-Band Microwave Radiometer Payload of the FSSCat Mission" *Remote Sens.* 13, no. 1: 121.

[5] A. Alonso-Arroyo, V. U. Zavorotny and A. Camps, "Sea Ice Detection Using U.K. TDS-1 GNSS-R Data," in IEEE Transactions on Geoscience and Remote Sensing, vol. 55, no. 9, pp. 4989-5001, Sept. 2017, doi: 10.1109/TGRS.2017.2699122.

[6] Q. Yan, W. Huang and C. Moloney, "Neural Networks Based Sea Ice Detection and Concentration Retrieval From GNSS-R Delay-Doppler Maps," in *IEEE Journal of Selected Topics in Applied Earth Observations and Remote Sensing*, vol. 10, no. 8, pp. 3789-3798, Aug. 2017, doi: 10.1109/JSTARS.2017.2689009.

[7] EUMETSAT OSI SAF, "Ocean and Sea Ice". Url: http://www.osi-saf.org/. [Accessed 22 12 2020]

[8] ECMWF, "European Centre for Medium-Range Weather Forecast". Url: https://www.ecmwf.int/ [Accessed 22 12 2020]

[9] M.J. Brodzik, B. Billingsley, T. Haran, B. Raup, M.H. Savoie, 2012. "EASE-Grid 2.0: Incremental but Significant Improvements for Earth-Gridded Data Sets" *ISPRS Int. J. Geo-Inf.* 1, no. 1: 32-45.

[10] Meier, W. and Stewart, J. "Assessing uncertainties in sea ice extent climate indicators." in *Environmental Research Letters*. 2018. 14. 10.1088/1748-9326/aaf52c.